Available online at www.sciencedirect.com

ScienceDirect

journal homepage: www.elsevier.com/locate/he

Doping of nitrogen into biomass-derived porous carbon with large surface area using N_2 non-thermal plasma technique for high-performance supercapacitor

Long Wu [a,b,*], *Yimeng Cai* [a], *Shizhe Wang* [a], *Zhanyong Li* [a,b]

[a] *Tianjin Key Laboratory of Integrated Design and On-line Monitoring for Light Industry & Food Machinery and Equipment, College of Mechanical Engineering, Tianjin University of Science & Technology, Tianjin, 300222, China*

[b] *International Joint Research Center of Low-Carbon Green Process Equipment, Tianjin, 300222, China*

HIGHLIGHTS

- Lilac and lotus seedpods were used to prepare porous carbons for supercapacitor electrodes.
- The obtained porous carbon achieves large surface areas up to 3040 m^2/g.
- Plasma modification enhances supercapacitor performances of obtained carbon electrodes.
- Lilac-derived carbon after plasma modification exhibits high capacitance of 342.5 F/g.
- Lotus seedpods-derived carbon after plasma modification exhibits high capacitance of 332.1 F/g.

GRAPHICAL ABSTRACT

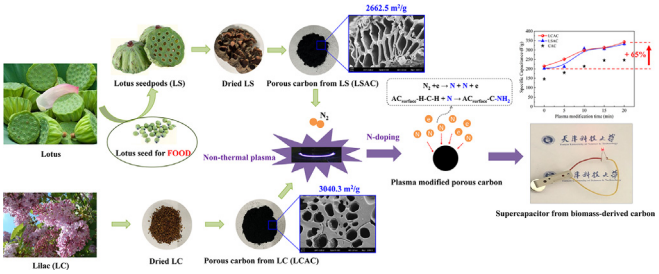

ARTICLE INFO

Article history:
Received 19 August 2020
Received in revised form
1 October 2020
Accepted 5 October 2020
Available online xxx

Keywords:
Biomass
Porous carbon

ABSTRACT

A novel and facile modified method using non-thermal plasma is proposed to insert N active sites into biomass-derived porous carbon as high-performance electrode materials for supercapacitor. Large surface areas up to 3040.3 and 2662.5 m^2/g with mesopore-dominant hierarchical porous carbons are produced from biomass of lilac and lotus seedpods via KOH activation, respectively. The lilac and lotus seedpods derived porous carbon electrodes present good specific capacitances of 214.5 and 201.1 F/g, respectively. N_2 non-thermal plasma modification successfully increases N-containing groups on lilac and lotus seedpods derived porous carbons, where the corresponding N atomic contents are increased by 10.2 and 3.6 times, respectively. As supercapacitor electrodes, their specific capacitances are improved greatly after plasma modification and up to 342.5 F/g (increased

* *Corresponding author*. Tianjin Key Laboratory of Integrated Design and On-line Monitoring for Light Industry & Food Machinery and Equipment, College of Mechanical Engineering, Tianjin University of Science & Technology, Tianjin 300222, China.
E-mail address: wulong@tust.edu.cn (L. Wu).

https://doi.org/10.1016/j.ijhydene.2020.10.037

Please cite this article as: Wu L et al., Doping of nitrogen into biomass-derived porous carbon with large surface area using N_2 non-thermal plasma technique for high-performance supercapacitor, International Journal of Hydrogen Energy, https://doi.org/10.1016/j.ijhydene.2020.10.037

N_2 plasma
Nitrogen-doping
Supercapacitor

by 59.7%) and to 332.1 F/g (increased by 65.2%) at 0.5 A/g in 6 M KOH electrolyte with excellent cycling stability of 85.2% and 95.4% at 10 A/g after 5000 cycles, respectively.

Introduction

The demand for clean and renewable energy is becoming increasing urgent due to the excessive and consumption of fossil energy and growing environmental problems. In order to solve the problems of uneven regional distribution in renewable energy and unstable energy sources, the development of environmentally friendly and high-performance energy storage device has been attracted considerable attention [1].

Electric double-layer capacitors (EDLCs) are one of most promising energy storage devices, owing to they can meet the energy storage needs in many renewable energy application conditions, such as energy storage systems for solar and wind power generation, power energy storage device etc [2]. Electrode material is one of most important factors which affect the electrochemical performance of EDLCs. Currently, the main materials used as electrodes for EDLCs include metal compounds, conductive polymers and carbon materials [1]. Among them, porous carbons have been considered promising electrode material candidates for EDLCs due to their large specific surface area, high electric conductivity, easy availability and good capacitive performances [3]. Traditional porous carbon materials were mainly produced from fossil fuel such as coal which is non-renewable resource. As a result, reuse and conversion of biomass into valuable porous carbon materials have attracted increasing attention due to its natural abundant, eco-friendly renewable resources, low cost and environmental sustainability, in particular for "waste-to-wealth" purpose [1,4–8]. Most processes for producing porous carbon materials derived from biomass is carbonization at high temperatures following by designed activation process such as physical activation with steam (or CO_2) and chemical treatment with chemical reagent ($ZnCl_2$, H_3PO_4, NaOH and KOH etc). For example, Zhang et al. [9] prepared a porous carbon with surface area of 1610 m^2/g and specific capacitance of 174 F/g at 0.5 A/g derived from lotus stem via carbonation in N_2. A capacitance of 206 F/g at 0.1 A/g was obtained in porous carbon derived from shrimp shell with surface area of 725.6 m^2/g by H_3PO_4 activation [10]. Zhao et al. [4] produced a 3D porous carbon with surface area of 1911 m^2/g specific capacitance of 208 F/g at 0.5 A/g via KOH activation using rose as raw materials. High specific surface area with hierarchically porous structure of porous carbon is an important factor affects the high-performance of EDLCs [11]. Choosing suitable biomass precursors and activation processes can produce porous carbon with high surface areas and large pore volumes. It is reported that the micropore dominant porous carbon are not suitable for electrode material of EDLCs, due to the micropore (pore size < 2 nm) limits the rapid ion diffusion and transport especially at high current density [11]. Hence, porous carbon including reasonable distribution of micropores, mesopores (pore size of 2–50 nm) and macropores (pore size > 50 nm) can effectively utilize the pore surface area and accelerate ion transfer to improve the electrochemical performance [12].

Apart from hierarchical porous structure, the heteroatoms (such as N, O, P and S etc) and surface functional groups in porous carbon also play a critical role in electrode performance [13,14]. Among them, nitrogen heteroatoms in the porous carbon can improve the surface wettability, electronic conductivity and induce the pseudocapacitance, and thus promote the capacitance of supercapacitor [15,16]. Hence, nitrogen doping into biomass derived porous carbon has drawn more and more attention for enhancing the performance of supercapacitors. The traditional methods to introduce nitrogen into porous carbon are mainly dependent on the complicated post-synthesis treatment by using reaction nitrogen sources such as NH_3, HCN, nitric acid, urea and melamine etc [16,17]. However, these N-doping synthesis reactions are complex, time-consuming and consume much reaction nitrogen sources (expensive and toxic) which can cause the chemical pollution problems. The N-doping process will be more feasible if a facile and efficient non-chemical method is developed.

Plasma technique is an effective surface modification method for carbon-based materials. During plasma modification process, high-energy electrons and active radicals can be generated and thus insert heteroatoms and corresponding active sites into porous carbon. It has been reported that plasma modification can increase the N-containing or O-containing functional groups of carbon materials [18,19]. Especially, plasma modification method is environmentally friendly which does not need chemical solution compared to the chemical treatment process. Although plasma modification for porous carbon is an effective and promising method,

Abbreviations

CAC	Commercial activated carbon
CV	Cyclic voltammetry
DBD	Dielectric barrier discharge
EDLCs	Electric double-layer capacitors
EIS	Electrochemical impedance spectrometry
GCD	Galvanostatic charge-discharge
LC	Lilac
LS	Lotus seedpods
LCAC	Lilac derived activated carbon
LSAC	Lotus seedpods derived activated carbon
PTFE	Poly-tetrafluoroethylene
SEM	Scanning electron microscopy
XPS	X-ray photoelectron spectroscopy
XRD	X-ray diffraction

Please cite this article as: Wu L et al., Doping of nitrogen into biomass-derived porous carbon with large surface area using N_2 non-thermal plasma technique for high-performance supercapacitor, International Journal of Hydrogen Energy, https://doi.org/10.1016/j.ijhydene.2020.10.037

no researchers have tried to use it for N-doping to improve supercapacitor performance. Therefore, this study is first time to introduce N_2 non-thermal plasma modification for doping of N into biomass-derived porous carbon as electrode materials to better supercapacitor performance. N_2 is a non-toxic gas and very cheap which can be easily produced. Importantly, no pollutant emission will be produced during N_2 plasma modification process.

In this study, two biomass precursors of lilac and lotus seedpods were used to produce the hierarchical porous carbons via a simple two-step method including carbonization and KOH activation. Lilac is widely grown in temperate areas of the world. Once lilac fall from the tree and they are literally of no economical value. Lotus is widely planted in the world, especially in the south of China, and the total planting area of lotus is about 330,000 ha. The lotus seed in the lotus is a typical and delicious food, while the lotus seedpods are always discarded as wastes. Lilac and lotus seedpods are renewable biomass, easily obtained and abundant available in large quantity, which are promising biomass carbon precursor for porous carbon materials. After activation, the obtained porous carbons achieved large specific surface areas up to 3040.3 (lilac-derived) and 2662.5 m^2/g (lotus seedpods-derived) with mesopore-dominant hierarchical porous structures. Then, the obtained biomass derived porous carbons were further modified by using N_2 non-thermal plasma generated by the dielectric barrier discharge (DBD). The N heteroatoms in the prepared porous carbons increased greatly after plasma modification and thus significantly promoted the supercapacitor performances. Herein, the low-cost hierarchical micro-meso biomass-derived porous carbons with doping of N for high-performance supercapacitors were successfully obtained. The effects of plasma modification on textural and electrochemical performance of the as-prepared porous carbon materials are discussed in detail.

Experimental

Preparation of activated carbon

Raw materials

The lotus seedpods (LS, without seed) and lilac (LC) used in this study were obtained from local farms in Jiangsu and Jilin Province, China, respectively. They were washed with deionized water to remove impurities. Afterwards, they were dried at 105 °C in oven for 12 h.

Preparations of lotus seedpods and lilac derived activated carbons

A 20.0 g of LS (as well as LC) were placed in a quartz boat and located at the center core of the horizontal electrical heating furnace (GSL-1700X, Hefei Kejing Materials Technology Co., Ltd., China). The temperature of furnace was first increased from room temperature (25 °C) to 500 °C with heating rate of 10 °C/min under a highly pure N_2 flow (100 ml/min, 99.99%), and held at 500 °C for 2 h for carbonization process. Thereafter, the carbonized LS (as well as carbonized LC) were mixed with KOH with mass ratio for carbonized LS (or carbonized LC)/KOH (solid) of 1:3. Then, the mixture powder was placed in the electrical heating furnace and the temperature of furnace was first increased from room temperature to 800 °C with heating rate of 10 °C/min under a highly pure N_2 flow (100 ml/min, 99.99%), and kept at 800 °C for 2 h for activation process. The obtained product was washed with diluted HCl solution and distilled water until the solution achieved neutral pH and then dried for 12 h at 105 °C. Then the LS (as well as LC) derived activated carbon (LSAC) was obtained, they were named as LSAC and LCAC, respectively. During carbonization process, the yields of obtained carbonized LS and carbonized LC were 40% (±1.6%) and 26% (±1.2%), respectively. During KOH activation process, the yields of obtained LSAC and LCAC were 66% (±1.7%) and 63% (±1.5%), respectively. In addition, a commercial activated carbon (derived from coconut shell, Kurary Company, Japan) for supercapacitor electrode was used for comparison and named as CAC.

Plasma modification process

The experimental setup of N_2 non-thermal plasma modification is presented in Fig. 1. The non-thermal plasma was generated by using a dielectric barrier discharge reactor (DBD-100A, CTP-2000K, Suman Corporation, China) via an alternating current with a 10 kHz audio-frequency and 3 kV peak voltage. A detailed description of the experimental setup can be found in Wu et al. [19,20], so only a brief description is given here. Pure N_2 (99.9%, vol. base) with 20 ml/min was introduced into the plasma modification reactor under room temperature and atmospheric pressure. The 1.0 g AC sample (LSAC or LCAC) were dispersed uniformly in the DBD plasma reactor. The AC samples were modified by N_2 non-thermal plasma for 5 min (named as LSAC-P5 or LCAC-P5), 10 min (LSAC-P10 or LCAC-P10), 15 min (LSAC-P15 or LCAC-P15) and 20 min (LSAC-P20 or LCAC-P20), respectively. All samples showed a slight weight loss (less than 1%), which could be negligible.

Characterization

Morphological features of AC samples before and after plasma modification were characterized by scanning electron microscopy (SEM, sigma 300, ZEISS, Germany). The crystal structures of AC samples were characterized by X-ray diffraction (XRD) in the 2θ range from 10 to 80° with Cu-Kα radiation. Raman scattering spectra of the AC samples were measured to determine the graphitic quality on a LabRAM HR800 (Horiba, Japan). The textural properties of the AC samples were characterized by measuring N_2 adsorption-desorption isotherms at 77 K (ASAP2460, Micromeritics, USA). X-ray photoelectron spectroscopy (XPS) was used to examine the surface bindings of the AC samples with surface excitation at 1253 eV by an Mg X-ray source (EscaLab 250Xi, Thermo Fisher Scientific). The XPS spectra were calibrated by setting the binding energy of C_{1s} at 285 eV.

Preparation of electrodes

The working electrodes were prepared by mixing the prepared AC samples with binder poly-tetrafluoroethylene (PTFE) and carbon black with the weight ratio of 8:1:1 in the absolute ethanol to form a slurry. Nickel-foam was used as current collector. The slurry was uniformity coated onto the nickel-

Please cite this article as: Wu L et al., Doping of nitrogen into biomass-derived porous carbon with large surface area using N_2 non-thermal plasma technique for high-performance supercapacitor, International Journal of Hydrogen Energy, https://doi.org/10.1016/j.ijhydene.2020.10.037

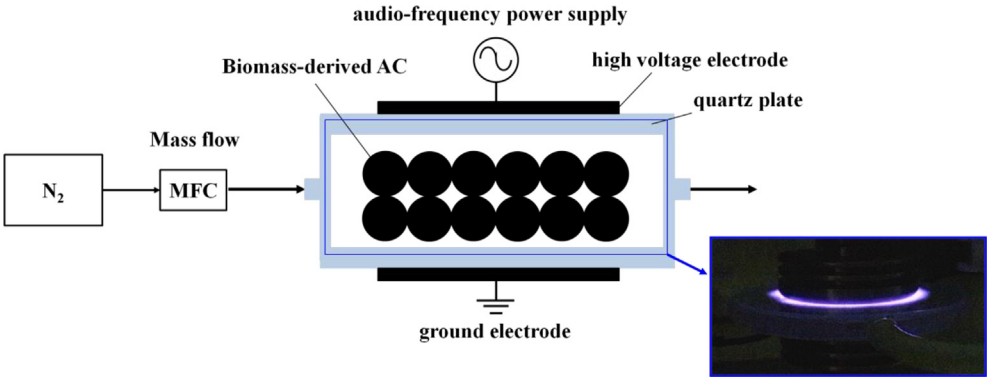

Fig. 1 – Schematic diagram of the N_2 non-thermal plasma modification system.

foam and pressed at 10 MPa, and then dried at 100 °C for 12h in a vacuum oven. The working electrodes had a coating area of 1 cm^2 (1 cm × 1 cm) and the AC sample mass on each electrode was about 3 mg.

Electrochemical measurement

The electrochemical capacitive performances of samples were conducted on a CHI660E electrochemical workstation (Shanghai CH Instrument Company, China). A three-electrode configuration, using 6 M KOH as the electrolyte, was constructed to evaluate the supercapacitive performance of the prepared electrode samples. The electrochemical measurements including galvanostatic charge-discharge (GCD), cyclic voltammetry (CV) and electrochemical impedance spectrometry (EIS). In the three-electrode system, a platinum plate and a calomel electrode were used as the counter electrode and reference electrode, respectively.

According to the GCD curves, the specific capacitance of the AC sample was calculated based on the following equation [21]:

$$C_m = \frac{I \times \Delta t}{\Delta V \times m} \quad (1)$$

where C_m is the specific capacitance (F/g), I corresponds to the applied discharge current (A), Δt denotes the time period of full discharge (s), ΔV is the voltage change windows (V), and m is the AC sample mass on the electrode surface (g).

All the experiments were repeated at least three times to obtain repeatable results. The error bars for measurements were calculated using the standard deviation.

Results and discussion

SEM and BET analysis

The SEM images of LCAC and LSAC samples before and after plasma modification are shown in Fig. 2. Both of LCAC and LSAC had well-developed porous structures, where numerous pores are distributed on surface of samples. The pores of LCAC are roughly circular in shape, whereas the pores of LSAC are shown as the rectangle. After plasma modification, although the LCAC-P20 (as well as LSAC-P20) still had porous structure, the surface morphology was seriously destroyed and became rougher with a lot of new created pores. Moreover, many interconnected pores were observed on the surface of LCAC-P20 and LSAC-P20, respectively. These phenomena can be attributed to the etching effect caused by plasma [22]. During plasma modification process, the high-energy particles bombarded the surface of AC samples which destroyed the original pore structure, broken the pore wall and generated new pores. The porous structure of AC samples is good for store a large amount of charge and is in favor of improving the electrochemical performances. Moreover, the interconnected pore structure can be beneficial for AC samples to provide transport channels and then improve the electrolyte ions transfer [23].

Nitrogen adsorption/desorption isotherms and pore size distributions of LCAC and LSAC samples before and after plasma modification are shown in Fig. 3. It can be seen that, the prepared AC samples (LCAC, LCAC-P20, LSAC and LSAC-P20) exhibited both type-I and type-IV isotherms according to the definition of IUPAC. This indicates that the pore structure of the prepared AC samples combined the micropores and mesopores. Moreover, the pores in the LCAC and LCAC-P20 mainly ranged over 0.5–3.5 nm (including micropores located from 0.5 to 2 nm and mesopores located from 2 to 3.5 nm), whereas the pores in LSAC and LSAC-P20 mainly range over 1.8–4 nm (including micropores located from 1.8 to 2 nm and mesopores located from 2 to 4 nm). It can be seen from Table 1, the average pore size (d_{pore}) of LCAC was 2.018 nm, which slightly increased to 2.024 nm after plasma modification (LCAC-P20). Whereas the average pore size of LSAC was 2.34 nm, which slightly decreased to 2.3 nm after plasma modification. The specific surface areas of LCAC and LSAC are 3040.3 m^2/g and 2662.5 m^2/g, respectively, indicating that lotus seedpods and lilac are promising biomass precursors to prepare the activated carbon with high surface area and well-developed porous structures. After plasma modification, the specific surface areas of LCAC-P20 and LSAC-P20 slightly decreased to 2961.7 m^2/g and 2514.2 m^2/g, respectively. For LCAC sample, after plasma modification, the micropores surface area, mesopores surface area, micropores volume, mesopores volume and total pore volume slightly decreased to 1021.8 m^2/g, 1939.9 m^2/g, 0.432 cm^3/g, 0.917 cm^3/g and 1.349 cm^3/g, respectively. For LSAC sample, after plasma modification, the micropores surface area and micropores

Please cite this article as: Wu L et al., Doping of nitrogen into biomass-derived porous carbon with large surface area using N_2 non-thermal plasma technique for high-performance supercapacitor, International Journal of Hydrogen Energy, https://doi.org/10.1016/j.ijhydene.2020.10.037

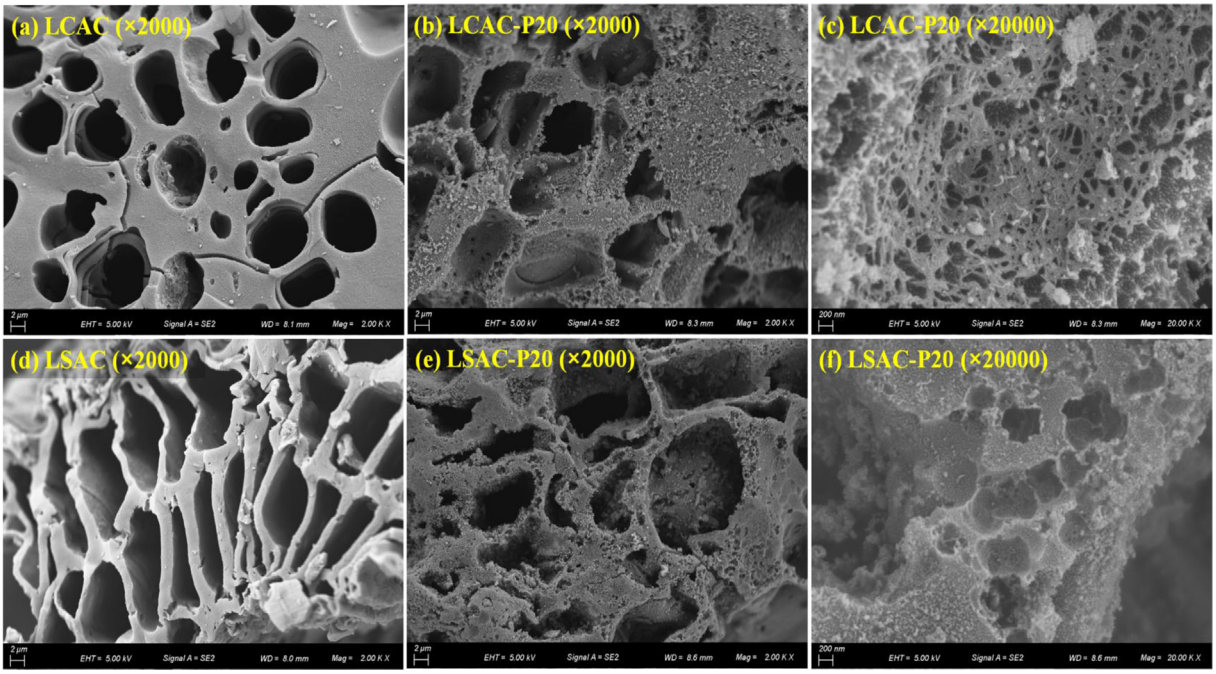

Fig. 2 – SEM images of LCAC (a) and LSAC (d), and plasma modified samples LCAC-P20 (b, c) and LSAC-P20 (e, f).

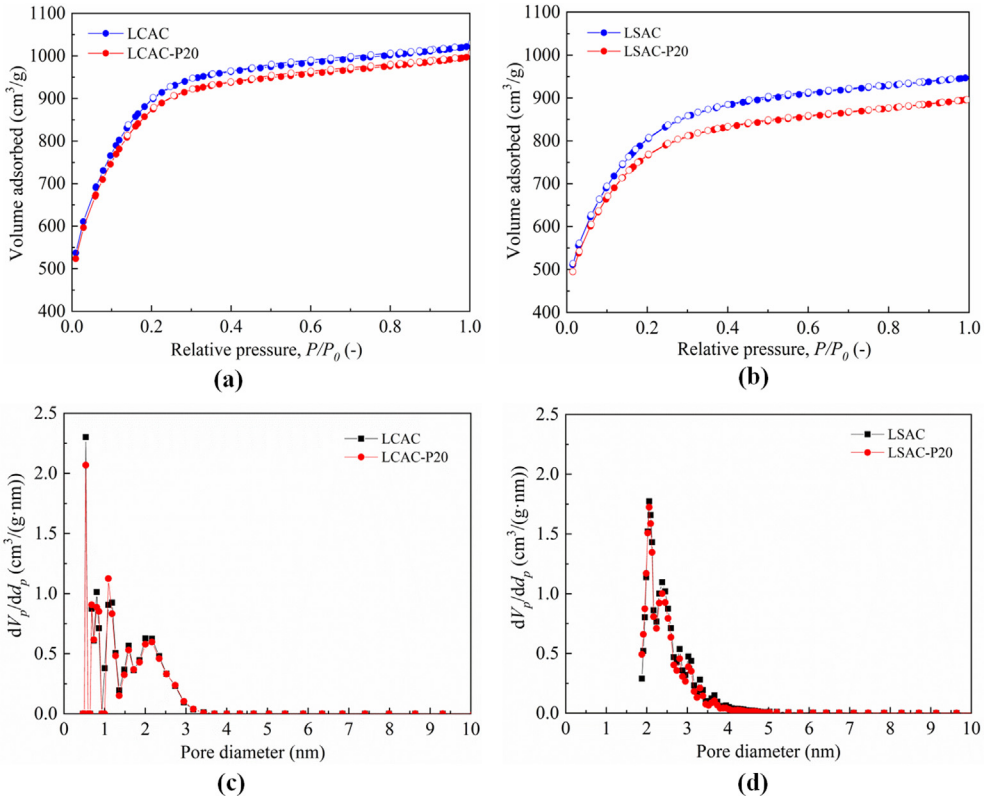

Fig. 3 – N_2 adsorption-desorption isotherms of LCAC vs. LCAC-P20 (a), and LSAC vs. LSAC-P20 (b); Pore size distribution of LCAC vs. LCAC-P20 (c), and LSAC vs. LSAC-P20 (d).

volume increased to 541.4 m^2/g, and 0.321 cm^3/g, respectively, whereas the mesopores surface area, mesopores volume and total pore volume decreased to 1972.8 m^2/g, 0.581 cm^3/g and 0.902 cm^3/g, respectively. These phenomena can be ascribed to the plasma etching effect, which led to the collapse, merging and new formation of micro/meso-pores. These results are consistent with the SEM results (Fig. 2). Impressively, the mesopores volumes in total pores volumes of LCAC, LCAC-

Please cite this article as: Wu L et al., Doping of nitrogen into biomass-derived porous carbon with large surface area using N_2 non-thermal plasma technique for high-performance supercapacitor, International Journal of Hydrogen Energy, https://doi.org/10.1016/j.ijhydene.2020.10.037

P20, LSAC and LSAC-P20 were up to 64.4%–78.8%, indicating that mesopores dominated the pores distribution for prepared AC samples. Therefore, the LCAC, LCAC-P20, LSAC and LSAC-P20 samples exhibited the hierarchical porosity network of high-density mesopores in combination with micropores, which is beneficial to enhancing electrochemical process [24]. It is well known that micropores are important for the charge storage, while mesopores provide fast mass-transport of electrolytes and reduce ion transport resistance, which are in favor of improving the capacitive and rate performance in the supercapacitor application [25]. To sum up, plasma modification exhibited slightly negative effects on porous properties of LCAC and LSAC, respectively. Nevertheless, after plasma modification, the LCAC and LSAC samples still had large surface areas (more than 2500 m^2/g) with well-developed hierarchical micro-meso porous structures.

XRD and Raman analysis

X-ray diffraction patterns (XRD) and Raman spectroscopy are used for analyzing the structural features of the prepared AC samples. Fig. 4a–b and 4c-4d show the XRD and Raman spectrum of LCAC, LCAC-P20, LSAC and LSAC-P20, respectively. As shown in Fig. 4a-b, the AC samples exhibited a broad characteristic XRD peak at around 23° and a weak peak at around 43°, respectively, which correspond to (002) and (101) planes of graphite carbon. XRD results indicate that the prepared AC samples before and after plasma modification have amorphous structures [26]. As can be seen from the Raman spectrum shown in Fig. 4c-d, the two strong peaks at around 1337 cm^{-1} and 1597 cm^{-1} in the Raman spectra of prepared AC samples are the so-called D-band and G-band, respectively [27], which are the most intense features of graphitic carbon. It is known that, the D-band is relevant to the presence of disordered carbon structures, while the G-band corresponds to the graphite structure of sp^2 hybrid carbon atoms [28]. The appearance of G-band implies the presence of graphitic domains [29]. Therefore, the prepared AC samples would be beneficial for enhancing the electrical conductivity when used as porous carbon electrode of the supercapacitor. Furthermore, the intensity ratio of D-band to G-band (I_D/I_G) indicates the graphitization and disorder degree of the prepared AC samples [30]. The Raman spectra show that the plasma modification increased the ratios of I_D/I_G of LCAC and LSAC from 0.953 to 1.085 to 0.981 and 1.09, respectively. These increases in I_D/I_G imply an increase in defective sites due to the nitrogen inserted into the carbon support of LCAC-P20 and LSAC-P20 during plasma modification process [31,32]. These results confirm that the doping of N heteroatom into the prepared AC samples can be achieved by N_2 plasma modification. This is consistent with the XPS spectra results which shown in the next discussion (Fig. 5 and Table 2). Importantly, the presence of N heteroatom is important for the enhancement in electrochemical performances of LCAC-P20 and LSAC-P20 as they provide additional active sites and protons for improvement in the wettability and pseudocapacitance [33].

XPS analysis

XPS was used to analyze the changes in the chemical states on the surface of LCAC and LSAC before and after N_2-plasma modification. As shown in the XPS survey spectra of the prepared AC samples (Fig. 5a and b), only carbon, nitrogen and oxygen were observed on the surface of the prepared AC samples. As shown in Table 2, the oxygen atomic percentage showed slightly change before and after N_2 plasma modification, indicating N_2 plasma modification did not affect the oxygen content. It can be seen from XPS curves, the intensities of N1s of LCAC and LSAC were weak, whereas the intensities of N1s became strong after plasma modification. Moreover, the N1s intensities of LCAC-P20 and LSAC-P20 were stronger than LCAC-P5 and LSAC-P5, respectively. As shown in Table 2, the contents of nitrogen element of LCAC and LSAC are 0.21% and 0.53%, respectively. With increasing plasma modification time to 5 min, the contents of nitrogen element increased to 1.28% for LCAC samples and increased to 1.30% for LSAC samples, respectively. Further increases plasma modification time to 20 min, the contents of nitrogen element further increased to 2.36% for LCAC samples and increased to 2.46% for LSAC samples, respectively. The nitrogen element contents of LCAC and LSAC were 10.2 times and 3.6 times higher after N_2 plasma modification for 20 min. Fig. 5c and d shows the N1s spectrum of prepared AC samples. For LCAC and LSAC, no obvious peaks can be observed. In contrast, after N_2-plasma modification, optimal fitting can be achieved by deconvolution of three peaks at 400.7 eV, 399.6 eV and 398.5 eV for N1s spectrum, which correspond to the quaternary nitrogen (N-Q), pyrrolic nitrogen (N-5) and pyridinic nitrogen (N-6), respectively [34]. After plasma modification for 5 min, the atomic percentages of N-Q, N-5 and N-6 in LCAC increased to 0.34%, 0.53% and 0.41%, while increased to 0.46%, 0.65% and 0.19% for LSAC, respectively. Further increases plasma modification time to 20 min, the N-Q, N-5 and N-6 in LCAC further increased to 0.83%, 0.89% and 0.64%, while increased to 0.56%, 1.09% and 0.81% for LSAC, respectively. During plasma modification process, the N_2 can be dissociated into high-energy ions, such

Table 1 – Surface area and pore structure parameters of the prepared AC samples.

Sample	S_{BET} (m^2/g)	S_{micro} (m^2/g)	S_{meso} (m^2/g)	C_{meso} (%)	V_{total} (cm^3/g)	V_{micro} (cm^3/g)	V_{meso} (cm^3/g)	W_{meso} (%)	d_{pore} (nm)
LCAC	3040.3	1082.3	1958.0	64.4%	1.419	0.488	0.931	65.6%	2.018
LCAC-P20	2961.7	1021.8	1939.9	65.5%	1.349	0.432	0.917	68.0%	2.024
LSAC	2662.5	301.4	2361.1	88.7%	0.990	0.210	0.780	78.8%	2.340
LSAC-P20	2514.2	541.4	1972.8	78.5%	0.902	0.321	0.581	64.4%	2.300

Note: S_{BET} is total BET specific surface area; S_{micro} is micropores specific surface area; S_{meso} is mesopores specific surface area; C_{meso} is contribution of S_{meso} to S_{BET}; V_{total} is total pore volume; V_{micro} is micropores volume; V_{meso} is mesopores volume ($V_{meso} = V_{total} - V_{micro}$); W_{meso} is contribution of V_{meso} to V_{total}; d_{pore} is average pore size.

Please cite this article as: Wu L et al., Doping of nitrogen into biomass-derived porous carbon with large surface area using N_2 non-thermal plasma technique for high-performance supercapacitor, International Journal of Hydrogen Energy, https://doi.org/10.1016/j.ijhydene.2020.10.037

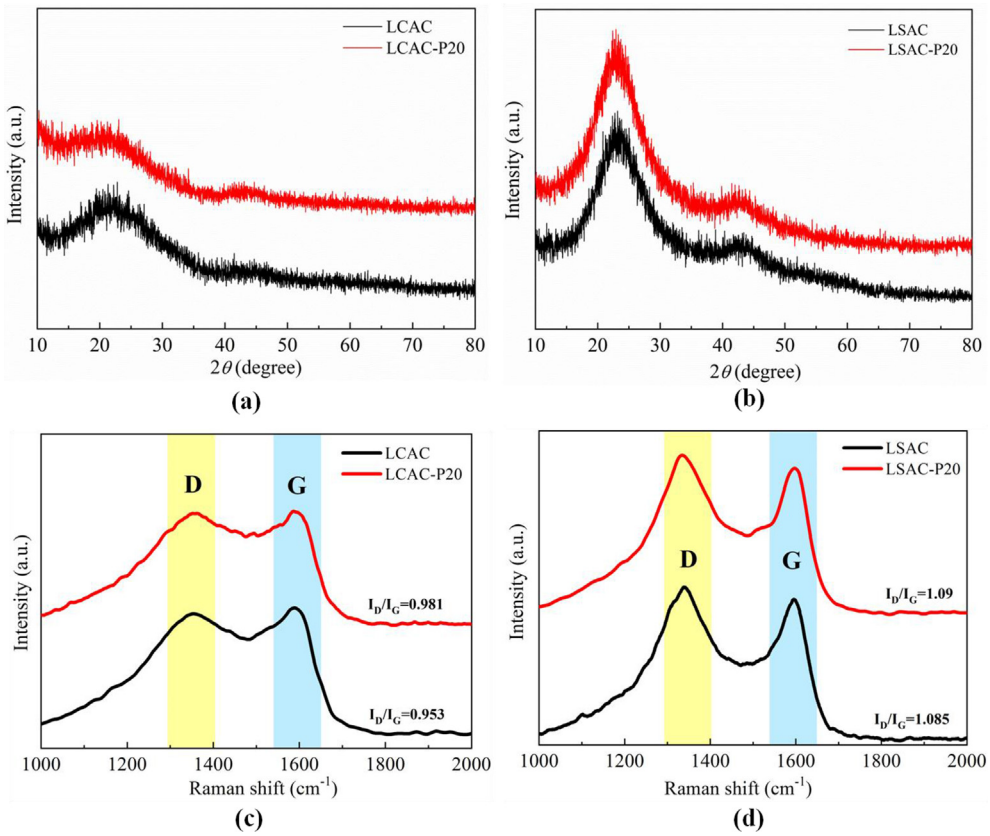

Fig. 4 – XRD patterns of LCAC vs. LCAC-P20 (a) and LSAC vs. LSAC-P20 (b); Raman spectrum of LCAC vs. LCAC-P20 (c) and LSAC vs. LSAC-P20 (d).

as N and N_2^+ etc. These ions are powerful and highly reactive which can easily react with the molecules of AC surface and generate N-containing functional groups [18]. The possible pathways for the N-containing groups formation on AC surface during N_2 plasma modification process can be described as follows:

$$N_2 + e \rightarrow N + N + e \quad (2)$$

$$N_2 \rightarrow N_2^+ + e \quad (3)$$

$$AC_{surface}\text{-}H\text{-}C\text{-}H + N \rightarrow AC_{surface}\text{-}C\text{-}NH_2 \quad (4)$$

Herein, N_2 plasma modification can result in an increase on N content of prepared AC samples. It is known that, due to N-5 has excellent electron-donor properties, fast charge fluxility and N-6 can provide the electron pairing with π-conjugated rings [24], N-5 and N-6 are the key bonds which can introduce pseudo-capacitance via the following reactions [17]:

$$AC{-}C{=}NH_2 + 2OH^- \leftrightarrow AC{-}C{=}NH + 2e^- + H_2O \quad (5)$$

$$AC{-}C{-}NH_2 + 2OH^- \leftrightarrow AC{-}C{-}NHOH + 2e^- + H_2O \quad (6)$$

Additionally, the presence of N-Q is in favor of efficient enhancing the electron transfer and electrical conductivity of porous carbon materials [12]. The appearance of these plentiful N-containing functional groups in AC samples after N_2 plasma modification will be highly beneficial to improve the electrochemical performances.

Electrochemical performance in 6 M KOH in a three electrode system

To explore the electrochemical performance of prepared AC samples as electrode materials for supercapacitors, cyclic voltammetry (CV), galvanostatic charge-discharge (GCD) and electrochemical impedance spectrometry (EIS) measurements were carried out in a three-electrode system with 6 M KOH as an electrolyte. Fig. 6a and Fig. 7a show the CV curves (at a scan rate of 10 mV/s) of LCAC and LSAC under N_2 plasma modification with different treatment times, respectively. Specially, a commercial activated carbon for supercapacitor electrode (derived from coconut shell, Kurary Company, Japan) named CAC was used for comparison. It can be seen that, all the shapes of CV curves of LCAC (as well as LSAC) and corresponding plasma modified AC samples presented approximately rectangular, which is the typical properties of EDLCs [35]. This indicates that the rapid ion transport can be operated in the prepared AC samples before and after plasma modification. The CV curve areas of prepared LCAC and LSAC samples were both larger than that of commercial activated carbon. Importantly, the CV curve areas of LCAC (as well as LSAC) further generally increased with plasma modification

Please cite this article as: Wu L et al., Doping of nitrogen into biomass-derived porous carbon with large surface area using N_2 non-thermal plasma technique for high-performance supercapacitor, International Journal of Hydrogen Energy, https://doi.org/10.1016/j.ijhydene.2020.10.037

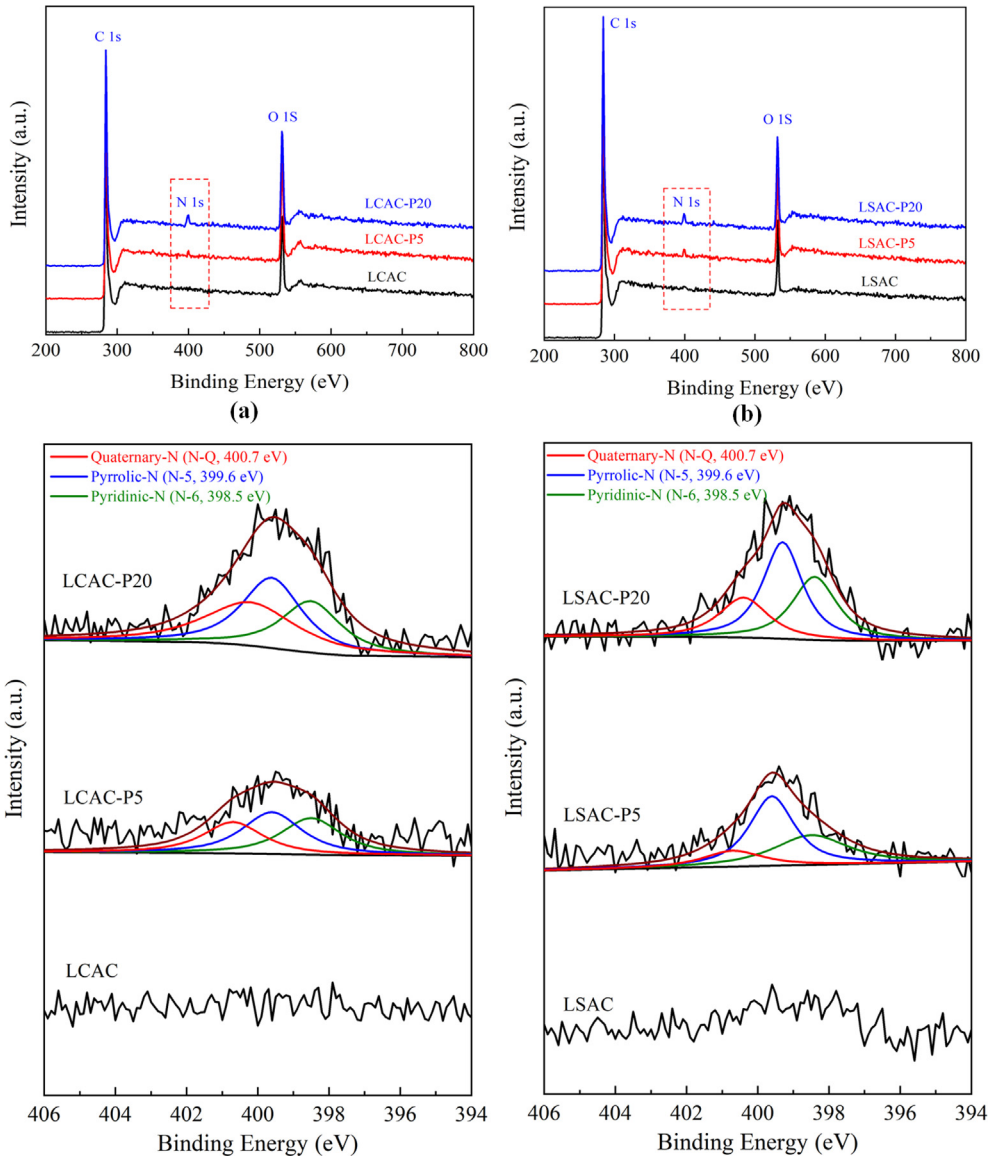

Fig. 5 – XPS survey spectra (a–b) and high-resolution scan of N1s spectra (c–d) for prepared porous carbon samples.

Table 2 – Functional groups and elemental composition of the prepared AC samples from XPS spectra.

Sample	Nitrogen content (atomic %)			Element content from XPS (atomic %)		
	N-Q	N-5	N-6	C	O	N
Electron binding energy (eV)	400.7	399.6	398.5			
LCAC	–	–	–	84.12	15.67	0.21
LCAC-P5	0.34	0.53	0.41	83.17	15.55	1.28
LCAC-P20	0.83	0.89	0.64	81.66	15.98	2.36
LSAC	–	–	–	87.06	12.41	0.53
LSAC-P5	0.46	0.65	0.19	86.53	12.17	1.30
LSAC-P20	0.56	1.09	0.81	85.21	12.33	2.46

Note: Quaternary-N (N-Q), Pyrrolic nitrogen (N-5), Pyridinic nitrogen (N-6).

from 5 to 20 min. This indicates that prepared LCAC and LSAC samples present higher specific capacitance than commercial AC electrode product, furthermore, plasma modification can further enhance the electrochemical performance of the prepared AC samples. Figs. 6b and 7b show the CV curves of LCAC-P20 and LSAC-P20 at different scan rates, respectively. No severe bending is observed for the CV curves of the LSAC-P20 with the scan rates increasing from 5 to 100 mV/s. For LCAC-P20, the CV curves maintain rectangular shape at scan rates from 5 to 50 mV/s, whereas a small distortion is observed when scan rate up to 100 mV/s. Nevertheless, these results indicate that the LCAC-P20 and LSAC-P20 have fast charge propagation performance and facile ion transport within their pore channels [36]. As discussed from results of BET analysis, the N_2 plasma modified LCAC and LSAC samples present the micro-meso hierarchical pore texture with high surface area (higher than 2500 m^2/g), which is accessible to electrolyte ions with low-resistance and achieve fast ion transfer.

Please cite this article as: Wu L et al., Doping of nitrogen into biomass-derived porous carbon with large surface area using N_2 non-thermal plasma technique for high-performance supercapacitor, International Journal of Hydrogen Energy, https://doi.org/10.1016/j.ijhydene.2020.10.037

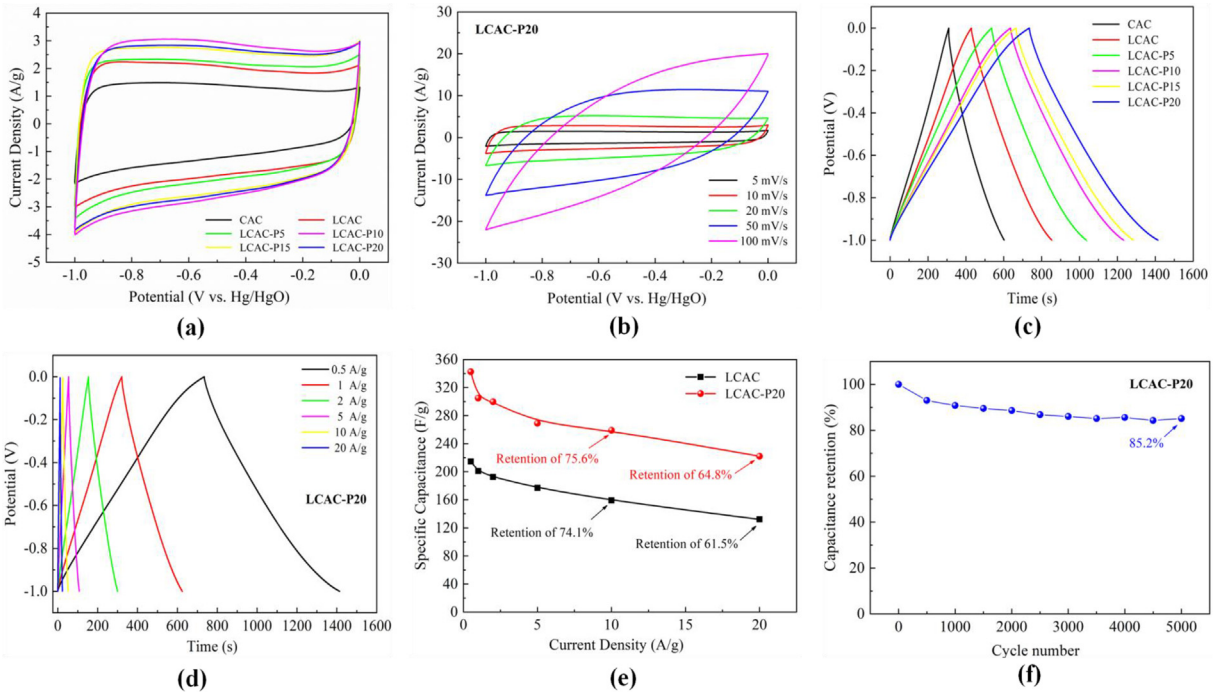

Fig. 6 – Electrochemical performance of LCAC and plasma modified LCAC in a three electrode configuration: (a) CV curves at a scan rate of 10 mV/s; (b) CV curves at different scan rates from 5 to 100 mV/s; (c) Galvanostatic charge–discharge curves at 0.5 A/g; (d) Galvanostatic charge–discharge curves under different current densities from 0.5 to 20 A/g; (e) Specific capacitances at different charge-discharge current densities; (f) Cycling stability at 10 A/g.

Figs. 6c and 7c show the GCD curves at a current density of 0.5 A/g of LCAC and LSAC under N_2 plasma modification with different treatment times, respectively. All the whole GCD curves of LCAC (as well as LSAC) and corresponding plasma modified AC samples showed almost isosceles triangular shapes, indicating the high charge-discharge efficiency and ideal characteristics for EDLCs. Both of LCAC and LSAC presented a longer charge-discharge time than CAC. Moreover, the charge-discharge time of LCAC (as well as LSAC) generally increased with plasma modification time. The LCAC-P20 and LSAC-P20 have the longest charge-discharge time and thus the highest specific capacitance value, respectively. As shown in Fig. 8a, the specific capacitances of LCAC and LSAC at 0.5 A/g are 214.5 and 201.1 F/g, respectively, which are both substantially higher than CAC (146.3 F/g). This indicates that the prepared AC samples showed better performances than commercial electrode material. Thus we believed that the prepared ACs derived from biomass of lilac and lotus seedpods can have well potential for practical supercapacitor application. It is interesting to note that, with increasing plasma modification time, all the specific capacitances of LCAC, LSAC and CAC at 0.5 A/g increased gradually, and achieved 342.5, 332.1 and 246.5 F/g, respectively. N_2 plasma modification enhanced the electrochemical performances of LCAC, LSAC and CAC, and the specific capacitances significantly increased by 59.7%, 65.1% and 68.5%, respectively. Although N_2 plasma modification decreased the specific surface areas of prepared ACs, the incorporation of nitrogen into carbon materials after N_2 plasma modification can enhance the electrical conductivity, wettability, and contribute to a pseudocapacitive effect [37]. The net effects of these influences (BET surface area vs. nitrogen incorporation) is that specific capacitances of prepared AC samples significantly increased after N_2 plasma modification.

Figs. 6d and 7d show the GCD curves of LCAC-P20 and LSAC-P20 under different current densities from 0.5 to 20 A/g, respectively. It can be seen that the GCD curves of LCAC-P20 and LSAC-P20 retain isosceles triangular shapes in all current densities even when the current density is high as 20 A/g, indicating plasma modified samples have slight internal resistance and excellent electrochemical reversibility. LCAC and LSAC show the specific capacitances of 132 and 144.2 F/g at the current densities of 20 A/g, with retention ratio of 61.5% and 71.7%, respectively, compared to their specific capacitances at 0.5 A/g. Meanwhile, after N_2 plasma modification, LCAC-P20 and LSAC-P20 could even maintain the specific capacitances of 222 and 252 F/g at the high current densities of 20 A/g, respectively, which are much higher than most carbon electrode materials ever reported. The corresponding retention ratio for LCAC-P20 and LSAC-P20 were 64.8% and 75.9%, respectively, compared to their specific capacitances at 0.5 A/g (as shown in Figs. 6e and 7e). It is interesting to note that the retention ratios of LCAC and LSAC improved after N_2 plasma modification. Specially, LSAC and LSAC-P20 exhibited pretty high capacitance retention ratios that achieved up to 80.1% and 81.3% at the current density of 10 A/g, while LCAC and LCAC-P20 exhibited inferior retention ratio performances compared to the LSAC and LSAC-P20. Nevertheless, the retention ratios of LCAC and LCAC-P20 were still more than 70% at the current density of 10 A/g. The good capacitance retention ratio performances of LCAC, LSAC and

Please cite this article as: Wu L et al., Doping of nitrogen into biomass-derived porous carbon with large surface area using N_2 non-thermal plasma technique for high-performance supercapacitor, International Journal of Hydrogen Energy, https://doi.org/10.1016/j.ijhydene.2020.10.037

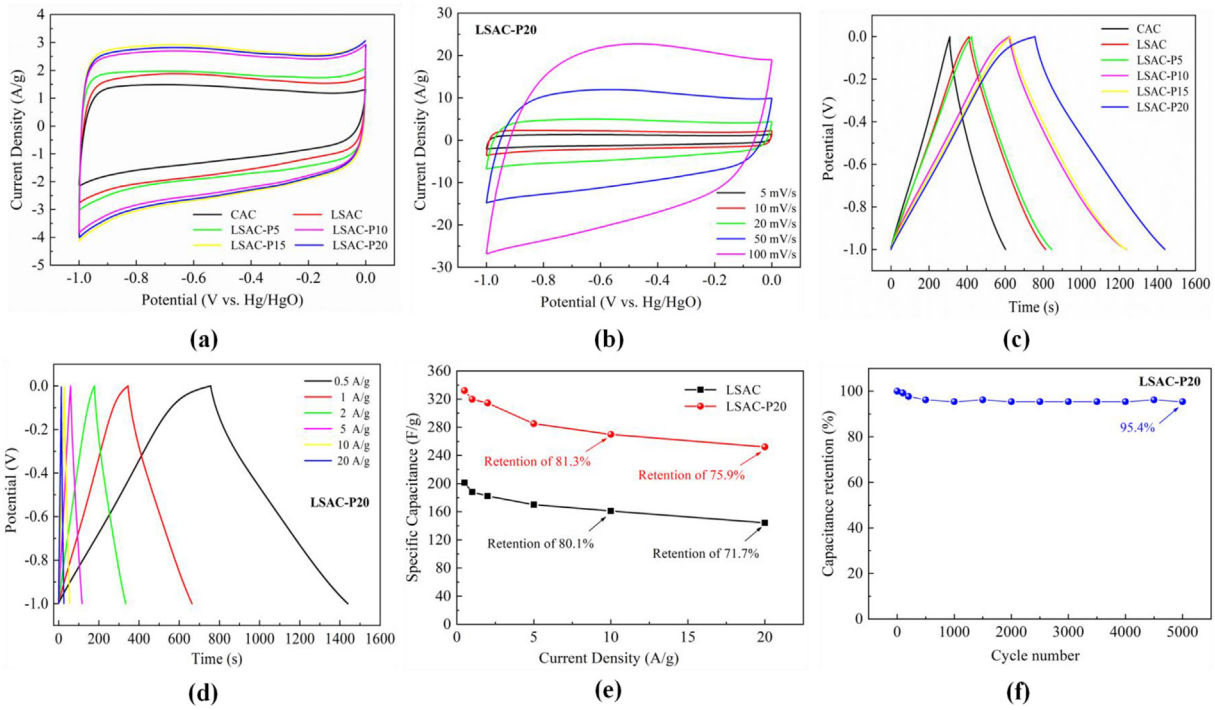

Fig. 7 – Electrochemical performance of LSAC and plasma modified LSAC in a three electrode configuration: (a) CV curves at a scan rate of 10 mV/s; (b) CV curves at different scan rates from 5 to 100 mV/s; (c) Galvanostatic charge–discharge curves at 0.5 A/g; (d) Galvanostatic charge–discharge curves under different current densities from 0.5 to 20 A/g; (e) Specific capacitances at different charge-discharge current densities; (f) Cycling stability at 10 A/g.

corresponding plasma modified samples can be ascribed to their hierarchical micro-meso porous structures with large surface areas.

The cyclic stability is an important factor of electrode materials for practical application of supercapacitors. Figs. 6f and 7f show the cyclic stability test results of LCAC-P20 and LSAC-P20 at a current density of 10 A/g under above-mentioned electrolytes. It can be seen that, the LCAC-P20 showed a good cyclic stability and kept 85.2% of its initial specific capacitance over 5000 cycles, while the LSAC-P20 exhibited long-term cycle stability of up to 95.4%, indicating the excellent electrochemical reproducibility.

The Nyquist plots of LCAC and LSAC before and after N_2 plasma modification measured by electrochemical impedance spectroscopy (EIS) in 6 M KOH over the frequency range of 100 kHz to 0.01 Hz are shown in Fig. 8b and c. It can be seen that Nyquist plots of the prepared samples can be divided into two parts: high frequency and low frequency regions, which exhibited the semicircle and straight line, respectively. This phenomena indicates a typical capacitive behavior [25]. In high frequency region, the equivalent series resistance (ESR) of LCAC-P20 electrode (0.51 Ω) and LSAC-P20 electrode (0.54 Ω) showed slightly changes compared to the LCAC electrode (0.54 Ω) and LSAC electrode (0.50 Ω), respectively, indicating N_2 plasma modification did not significantly affect the contact resistance of prepared AC sample electrodes. It is interesting to note that, the charge transfer resistances (the diameter of the semicircle) of LCAC-P20 electrode (1.0 Ω) and LSAC-P20 electrode (0.57 Ω) showed much smaller than LCAC electrode (1.8 Ω) and LSAC electrode (0.95 Ω), respectively. This can be ascribed to the nitrogen doping into the LCAC and LSAC electrodes after N_2 plasma modification which can help to enhance the surface wettability and electrical conductivity, and thus decreased the charge transfer resistances. Moreover, in low frequency regions, the Nyquist plots of LCAC and LSAC electrodes presented increasing slopes after plasma modification, indicating ion transportation properties were enhanced. The results of EIS further confirm that N_2 plasma modification promotes the capacitive performance of prepared AC samples.

To compare the capacitive performance of the prepared AC electrodes in this study, a summary of performances of other biomass derived carbon electrodes is listed in Table 3. It can be seen that, obtained AC electrodes derived from Lilac and Lotus seedpods showed better capacitive performances than electrodes using AC from lotus stem [9], Shrimp shells [10] and Coconut shell (Commercial electrode carbon). After N_2 plasma modification, the capacitive performances of obtained AC electrodes derived from Lilac and Lotus seedpods (as well as commercial electrode carbon) improved significantly. Importantly, the plasma modified lilac and lotus seedpods derived AC electrodes exhibited much higher capacitive performances than other reported AC electrodes under same measurement conditions [4,9,10,38–43].

Please cite this article as: Wu L et al., Doping of nitrogen into biomass-derived porous carbon with large surface area using N_2 non-thermal plasma technique for high-performance supercapacitor, International Journal of Hydrogen Energy, https://doi.org/10.1016/j.ijhydene.2020.10.037

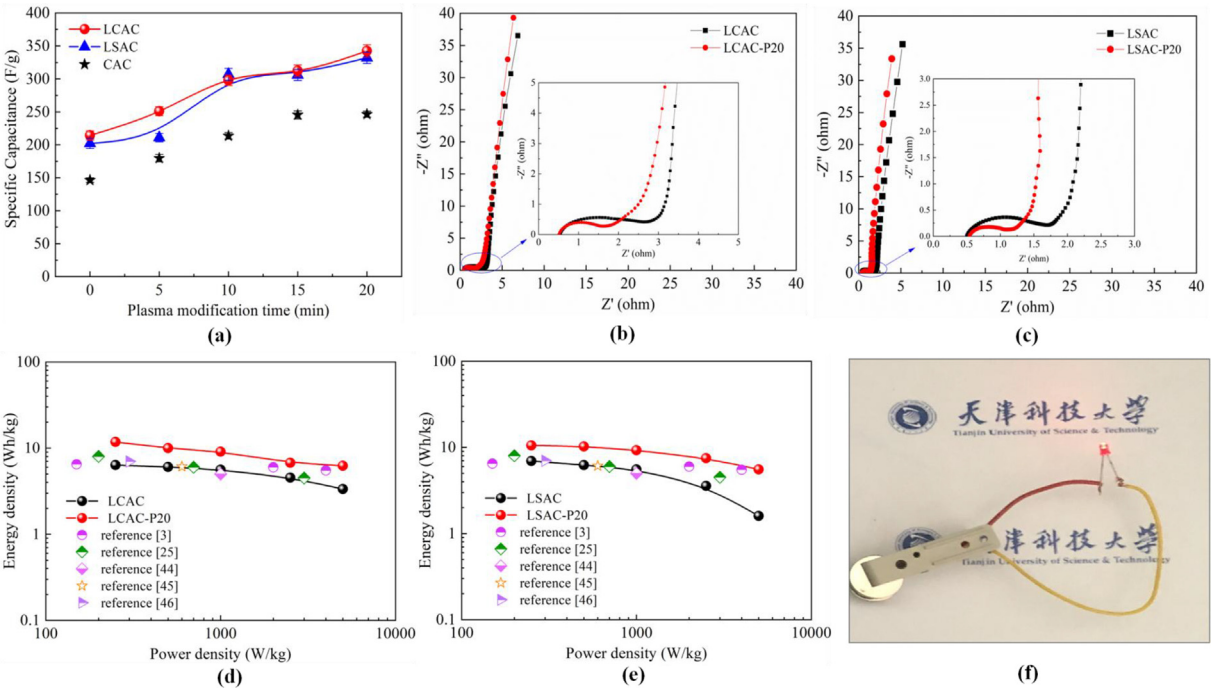

Fig. 8 – (a) Specific capacitances of LCAC, LSAC and CAC at 0.5 A/g under different plasma modification times; (b–c) Nyquist plots of LCAC and LSAC before and after N_2 plasma modification in 6 M KOH over the frequency range of 100 kHz to 0.01 Hz; (d–e) Ragone plots of LCAC and LSAC before and after N_2 plasma modification tested by using a two-electrode symmetric supercapacitor in 6 M KOH; (f) A LED powered with assembled organic electrolyte based supercapacitor by using LSAC-P20 as electrode material.

Electrochemical performance in 6 M KOH in a two electrode system

To validate the performances of prepared biomass-derived porous carbon electrodes, further tests were carried out by using a two-electrode symmetric supercapacitor in 6 M KOH. The Ragone plots of LCAC and LSAC before and after N_2 plasma modification are presented in Fig. 8d and e. The maximum energy densities of LCAC and LSAC based symmetric supercapacitor are 6.36 and 6.94 Wh/kg at 250 W/kg, respectively. After N_2 plasma modification, their energy densities significantly increased for each power density case. The high energy densities of 11.8 and 10.6 Wh/kg for LCAC-P20 and LSAC-P20 were achieved at 250 W/kg, respectively,

Table 3 – Summary of capacitive performances of biomass-derived carbon-based supercapacitor electrodes under three-electrode configuration.

Carbon type	Activation agent	S_{BET} (m^2/g)	Specific capacitance (F/g)	Measurement condition	Electrolyte	Reference
Rose derived carbon	KOH	1911	208	0.5 A/g	6.0 M KOH	[4]
lotus stem derived carbon	N_2	1610	174	0.5 A/g	6.0 M KOH	[9]
Shrimp shells derived carbon	H_3PO_4	725.6	175	0.5 A/g	6.0 M KOH	[10]
lotus receptacle derived carbon	H_2O_2	1015	340	0.5 A/g	3.0 M KOH	[38]
Perilla frutescens derived carbon	N_2	655	270	0.5 A/g	1 M Na_2SO4	[39]
Tremella derived carbon	KOH	1097	299	0.5 A/g	6.0 M KOH	[40]
Coconut shell based porous carbon	Steam	462.1	228	5 mV/s	6 M KOH	[41]
Moringa oleifera stems derived carbon	$ZnCl_2$/$FeCl_3$	2250	283	0.5 A/g	6 M KOH	[42]
Ginkgo shell derived carbon	KOH	1775	328	5 mV/s	6 M KOH	[43]
Commercial electrode carbon (Coconut shell based)	–	2100	146.3	0.5 A/g	6 M KOH	Kurary, Japan
Lilac derived carbon	KOH	3040.3	214.5	0.5 A/g	6 M KOH	**This study**
Lotus seedpods derived carbon	KOH	2662.5	201.1	0.5 A/g	6 M KOH	**This study**
Plasma modified Commercial electrode carbon	N_2 plasma	1943	246.5	0.5 A/g	6 M KOH	**This study**
Plasma modified lilac derived carbon	N_2 plasma	2961.7	342.5	0.5 A/g	6 M KOH	**This study**
Plasma modified lotus seedpods derived carbon	N_2 plasma	2514.2	332.1	0.5 A/g	6 M KOH	**This study**

Please cite this article as: Wu L et al., Doping of nitrogen into biomass-derived porous carbon with large surface area using N_2 non-thermal plasma technique for high-performance supercapacitor, International Journal of Hydrogen Energy, https://doi.org/10.1016/j.ijhydene.2020.10.037

and increased by 86% and 53% compared to the LCAC and LSAC. Even at high power densities of 5000 W/kg, LCAC-P20 and LSAC-P20 still can retain good energy densities of 6.3 and 5.6 Wh/kg (about 53% for each case of the capacitance retention). As shown in Fig. 8d and e, these values are better than most of the porous carbon materials reported in the literatures [3,25,44–46]. Furthermore, the device based on LSAC-P20 as electrode successfully powered 1.5 V red light emitting diode as shown in Fig. 8f. The CV, GCD and cycling stability test curves of LCAC-P20 and LSAC-P20 are shown in Figs. S1 and S2 (see supplementary material), respectively. It can be seen that, the CV and GCD shapes of LCAC-P20 (as well as LSAC-P20) presented approximately rectangular and isosceles triangular shapes, respectively, indicating a typical EDLCs behavior. As shown in Fig. 1S(d) and 2S(d), the cycling stabilities of LCAC-P20 and LSAC-P20 electrodes at 5 A/g still retained 96.2% and 89.8% after 5000 cycles, indicating the excellent cycling performances.

The favorable electrochemical performances of the LCAC and LSAC electrodes could be attributed to the hierarchically micro-meso porous structures with high surface areas. The further improvement of the electrochemical performance for N_2 plasma modified LCAC and LSAC electrodes are benefited from the nitrogen-doping and appearance of abundant nitrogen-containing functional groups. It can be concluded that N_2 plasma modification can insert N into the biomass-derived activated carbons and produced N-containing groups which can promote the electrochemical performance. The use of N_2 plasma modification technique can be considered a facile, efficient and environmentally friendly method for improving the electrochemical performance of biomass-derived AC electrode.

Conclusion

Mesopore-dominant hierarchical porous structures with large surface areas (up to 2662–3040 m^2/g) ACs were produced from biomass of lilac and lotus seedpods, and they show good specific capacitances of 214.5 and 201.1 F/g, respectively. A novel method using N_2 non-thermal plasma was firstly conducted to insert N active sites into biomass-derived porous carbon as electrode materials to promote the supercapacitor performance. After N_2 plasma modification, N atomic contents of lilac and lotus seedpods derived porous carbons were increased by 10.2 and 3.6 times, respectively, and the corresponding N-containing groups in obtained porous carbons were significantly increased. Consequently, the specific capacitances of lilac and lotus seedpods-derived porous carbon electrodes significantly increased to 342.5 F/g (increased by 59.7%) and to 332.1 F/g (increased by 65.2%), respectively. Meanwhile, lilac and lotus seedpods-derived porous carbon electrodes showed excellent cycling stability of 85.2% and 95.4% after 5000 cycles, respectively. From the results, N_2 plasma modification exhibits a facile and promising method to enhance the electrochemical performance of biomass-derived AC as supercapacitor electrode.

Declaration of competing interest

The authors declare that they have no known competing financial interests or personal relationships that could have appeared to influence the work reported in this paper.

Acknowledgements

The authors gratefully acknowledge the financial supports from the Tianjin Education Commission Research Project (2018KJ117).

Appendix A. Supplementary data

Supplementary data to this article can be found online at https://doi.org/10.1016/j.ijhydene.2020.10.037.

REFERENCES

[1] Wang J, Zhang X, Li Z, Ma Y, Ma L. Recent progress of biomass-derived carbon materials for supercapacitors. J Power Sources 2020;451:227794.
[2] Simon P, Gogotsi Y. Materials for electrochemical capacitors. Nat Mater 2008;7:845–54.
[3] Qu W, Xu Y, Lu A, Zhang X, Li W. Converting biowaste corncob residue into high value added porous carbon for supercapacitor electrodes. Bioresour Technol 2015;189:285–91.
[4] Zhao C, Huang Y, Zhao C, Shao X, Zhu Z. Rose-derived 3D carbon nanosheets for high cyclability and extended voltage supercapacitors. Electrochim Acta 2018;291:287–96.
[5] Azwar E, Mahari WAW, Chuah JH, Vo DVN, Ma NL, Lam WH, Lam SS. Transformation of biomass into carbon nanofiber for supercapacitor application – a review. Int J Hydrogen Energy 2018;43:20811–21.
[6] F HH, C L, G H, Y X, H J, W G, Y F, L H, F C, S YL. Walnut shell-derived hierarchical porous carbon with high performances for electrocatalytic hydrogen evolution and symmetry supercapacitors. Int J Hydrogen Energy 2020;45:443–51.
[7] Wang K, Xu M, Gu Z, Ahrenkiel P, Lee J, Gibbons W, Croat J, Fan Q. Pyrrole modified biomass derived hierarchical porous carbon as high performance symmetrical supercapacitor electrodes. Int J Hydrogen Energy 2016;41:13109–15.
[8] Golmohammadi F, Amiri M. Biomass-derived graphene-based nanocomposite: a facile template for decoration of ultrathin nickel–aluminum layered double hydroxide nanosheets as high-performance supercapacitors. Int J Hydrogen Energy 2020;45:15578–88.
[9] Zhang Y, Liu S, Zheng X, Wang X, Xu Y, Tang H, Kang F, Yang Q-H, Luo J. Biomass organs control the porosity of their pyrolyzed carbon. Adv Funct Mater 2017;27:1604687.
[10] Qu J, Geng C, Lv S, Shao G, Ma S, Wu M. Nitrogen, oxygen and phosphorus decorated porous carbons derived from shrimp shells for supercapacitors. Electrochim Acta 2015;176:982–8.
[11] Xia K, Gao Q, Jiang J, Hu J. Hierarchical porous carbons with controlled micropores and mesopores for supercapacitor electrode materials. Carbon 2008;46:1718–26.
[12] Quan H, Fan X, Wang W, Gao W, Dong Y, Chen D. Hierarchically porous carbon derived from biomass: effect of

mesopore and heteroatom-doping on electrochemical performance. Appl Surf Sci 2018;460:8–16.
[13] Li Z, Zhang L, Amirkhiz BS, Tan X, Xu Z, Wang H, Olsen BC, Holt CMB, Mitlin D. Carbonized chicken eggshell membranes with 3D architectures as high-performance electrode materials for supercapacitors. Advanced Energy Materials 2012;2:431–7.
[14] Demir M, Ashourirad B, Mugumya JH, Saraswat SK, Elkaderi HM, Gupta RB. Nitrogen and oxygen dual-doped porous carbons prepared from pea protein as electrode materials for high performance supercapacitors. Int J Hydrogen Energy 2018;43:18549–58.
[15] He D, Niu J, Dou M, Ji J, Huang Y, Wang F. Nitrogen and oxygen co-doped carbon networks with a mesopore-dominant hierarchical porosity for high energy and power density supercapacitors. Electrochim Acta 2017;238:310–8.
[16] Ma G, Yang Q, Sun K, Peng H, Ran F, Zhao X, Lei Z. Nitrogen-doped porous carbon derived from biomass waste for high-performance supercapacitor. Bioresour Technol 2015;197:137–42.
[17] Ferrero GA, Fuertes AB, Sevilla M. N-doped porous carbon capsules with tunable porosity for high-performance supercapacitors. J Mater Chem 2015;3:2914–23.
[18] Qayyum A, Zeb S, Naveed MA, Rehman NU, Ghauri SA, Zakaullah M. Optical emission spectroscopy of Ar–N2 mixture plasma. J Quant Spectrosc Ra 2007;107:361–71.
[19] Wu L, Shang Z, Zhu H, Li Z, Luo G, Yao H. Gas-phase mercury removal by modified activated carbons treated with Ar-O2 non-thermal plasma under different O2 concentrations. Int J Chem React Eng 2019;17.
[20] Wu L, Wan W, Shang Z, Gao X, Kobayashi N, Luo G, Li Z. Surface modification of phosphoric acid activated carbon by using non-thermal plasma for enhancement of Cu(II) adsorption from aqueous solutions. Separ Purif Technol 2018;197:156–69.
[21] Sun L, Tian C, Li M, Meng X, Wang L, Wang R, Yin J, Fu H. From coconut shell to porous graphene-like nanosheets for high-power supercapacitors. J Mater Chem 2013;1:6462–70.
[22] Winters HF, Coburn JW. Surface science aspects of etching reactions. Surf Sci Rep 1992;14:162–269.
[23] Yang J, Hu J, Zhu M, Zhao Y, Chen H, Pan F. Ultrahigh surface area meso/microporous carbon formed with self-template for high-voltage aqueous supercapacitors. J Power Sources 2017;365:362–71.
[24] Yang S, Wang S, Liu X, Li L. Biomass derived interconnected hierarchical micro-meso-macro- porous carbon with ultrahigh capacitance for supercapacitor. Carbon 2019;147:540–9.
[25] Sun F, Gao J, Liu X, Pi X, Yang Y, Wu S. Porous carbon with a large surface area and an ultrahigh carbon purity via templating carbonization coupling with KOH activation as excellent supercapacitor electrode materials. Appl Surf Sci 2016;387:857–63.
[26] Yang V, Senthil RA, Pan JQ, Khan A, Osman S, Wang LR, Jiang WC, Sun YZ. Highly ordered hierarchical porous carbon derived from biomass waste mangosteen peel as superior cathode material for high performance supercapacitor. J Electroanal Chem 2019;855.
[27] Senthilkumar ST, Selvan RK. Flexible fiber supercapacitor using biowaste-derived porous carbon. Chemelectrochem 2015;2:1111–6.
[28] Li YB, Zhang DY, Zhang YM, He JJ, Wang YL, Wang KJ, Xu YT, Li HX, Wang Y. Biomass-derived microporous carbon with large micropore size for high-performance supercapacitors. J Power Sources 2020;448.
[29] Jia R, Chen J, Zhao J, Zheng J, Chang S, Li L, Zhu Z. Synthesis of highly nitrogen-doped hollow carbon nanoparticles and their excellent electrocatalytic properties in dye-sensitized solar cells. J Mater Chem 2010;20.
[30] Gong YN, Li DL, Luo CZ, Fu Q, Pan CX. Highly porous graphitic biomass carbon as advanced electrode materials for supercapacitors. Green Chem 2017;19:4132–40.
[31] Shruthi TK, Saravana KM, Aswin PP, Naveen C. Graphene oxide aided structural tailoring of 3D N-doped amorphous carbon network for enhanced energy storage. RSC Adv 2015;5. 10.1039.C1035RA18494K.
[32] Wang HY, Zhou YF, Zhao Q, Zhang XL, Di LB. NH_3 plasma synthesis of N-doped activated carbon supported Pd catalysts with high catalytic activity and stability for HCOOH dehydrogenation. Int J Hydrogen Energy 2020;45:21380–91.
[33] Yang M, Zhong Y, Zhou X, Ren J, Su L, Wei J, Zhou Z. Ultrasmall MnO@N-rich carbon nanosheets for high-power asymmetric supercapacitors. J Mater Chem 2014;2:12519–25.
[34] Liu H, Song H, Chen X, Zhang S, Zhou J, Ma Z. Effects of nitrogen- and oxygen-containing functional groups of activated carbon nanotubes on the electrochemical performance in supercapacitors. J Power Sources 2015;285:303–9.
[35] Liu M, Gan L, Wei X, Zhao F, Fan X, Zhu D, Xu Z, Hao Z, Chen L. Nickel-Doped activated mesoporous carbon microspheres with partially graphitic structure for supercapacitors. Energy Fuel 2013;27:1168–73.
[36] Gao X, Xing W, Zhou J, Wang G, Zhuo S, Liu Z, Xue Q, Yan Z. Superior capacitive performance of active carbons derived from Enteromorpha prolifera. Electrochim Acta 2014;133:459–66.
[37] Xu G, Han J, Ding B, Nie P, Pan J, Dou H, Li H, Zhang X. Biomass-derived porous carbon materials with sulfur and nitrogen dual-doping for energy storage. Green Chem 2015;17:1668–74.
[38] Lu S, Jin M, Zhang Y, Niu Y, Gao J, Li CM. Chemically exfoliating biomass into a graphene-like porous active carbon with rational pore structure, good conductivity, and large surface area for high-performance supercapacitors. Advanced Energy Materials 2018;8:1702545.
[39] Liu B, Liu Y, Chen H, Yang M, Li H. Oxygen and nitrogen co-doped porous carbon nanosheets derived from Perilla frutescens for high volumetric performance supercapacitors. J Power Sources 2017;341:309–17.
[40] Chen D, Li L, Xi Y, Li J, Lu M, Cao J, Han W. Self-assembly of biomass microfibers into 3D layer-stacking hierarchical porous carbon for high performance supercapacitors. Electrochim Acta 2018;286:264–70.
[41] Misnon II, Zain NKM, Aziz RA, Vidyadharan B, Jose R. Electrochemical properties of carbon from oil palm kernel shell for high performance supercapacitors. Electrochim Acta 2015;174:78–86.
[42] Cai Y, Luo Y, Dong H, Zhao X, Xiao Y, Liang Y, Hu H, Liu Y, Zheng M. Hierarchically porous carbon nanosheets derived from Moringa oleifera stems as electrode material for high-performance electric double-layer capacitors. J Power Sources 2017;353:260–9.
[43] Jiang L, Yan J, Hao L, Xue R, Sun G, Yi B. High rate performance activated carbons prepared from ginkgo shells for electrochemical supercapacitors. Carbon 2013;56:146–54.
[44] He X, Ling P, Qiu J, Yu M, Zhang X, Yu C, Zheng M. Efficient preparation of biomass-based mesoporous carbons for supercapacitors with both high energy density and high power density. J Power Sources 2013;240:109–13.
[45] Le T, Yang Y, Huang Z, Kang F. Preparation of microporous carbon nanofibers from polyimide by using polyvinyl pyrrolidone as template and their capacitive performance. J Power Sources 2015;278:683–92.
[46] He X, Li R, Qiu J, Xie K, Ling P, Yu M, Zhang X, Zheng M. Synthesis of mesoporous carbons for supercapacitors from coal tar pitch by coupling microwave-assisted KOH activation with a MgO template. Carbon 2012;50:4911–21.

Please cite this article as: Wu L et al., Doping of nitrogen into biomass-derived porous carbon with large surface area using N_2 non-thermal plasma technique for high-performance supercapacitor, International Journal of Hydrogen Energy, https://doi.org/10.1016/j.ijhydene.2020.10.037